Biochimica et Biophysica Acta 1788 (2009) 333–344

Contents lists available at ScienceDirect

Biochimica et Biophysica Acta

journal homepage: www.elsevier.com/locate/bbamem

Interaction of an artificial antimicrobial peptide with lipid membranes

Lanlan Yu [a,b], Lin Guo [a], Jeak Ling Ding [c], Bow Ho [d], Si-shen Feng [e], Jonathan Popplewell [f], Marcus Swann [f], Thorsten Wohland [a,*]

[a] Department of Chemistry, National University of Singapore, 3 Science Drive 3, Singapore 117543, Singapore
[b] Department of Chemistry, Zhengzhou University, Zhengzhou 450001, PR China
[c] Department of Biological Sciences, National University of Singapore, 14 Science Drive 4, Singapore 117543, Singapore
[d] Department of Microbiology, National University of Singapore, 5 Science Drive 2, Singapore 117597, Singapore
[e] Division of Bioengineering, Chemical and Biomolecular Engineering, National University of Singapore, 10 Kent Ridge Crescents, Singapore 119260, Singapore
[f] Farfield Group, Farfield House, Electra Way, Crewe, CW1 6GU, UK

ARTICLE INFO

Article history:
Received 25 April 2008
Received in revised form 10 October 2008
Accepted 10 October 2008
Available online 25 October 2008

Keywords:
Antimicrobial peptide
Fluorescence correlation spectroscopy
Dual polarization interference
Langmuir–Blodgett trough
Langmuir film balance
Lipid vesicle
Supported bilayer

ABSTRACT

Antimicrobial peptides constitute an important part of the innate immune defense and are promising new candidates for antibiotics. Naturally occurring antimicrobial peptides often possess hemolytic activity and are not suitable as drugs. Therefore, a range of new synthetic antimicrobial peptides have been developed in recent years with promising properties. But their mechanism of action is in most cases not fully understood. One of these peptides, called V4, is a cyclized 19 amino acid peptide whose amino acid sequence has been modeled upon the hydrophobic/cationic binding pattern found in Factor C of the horseshoe crab (*Carcinoscorpius rotundicauda*). In this work we used a combination of biophysical techniques to elucidate the mechanism of action of V4. Langmuir–Blodgett trough, atomic force microscopy, Fluorescence Correlation Spectroscopy, Dual Polarization Interference, and confocal microscopy experiments show how the hydrophobic and cationic properties of V4 lead to a) selective binding of the peptide to anionic lipids (POPG) versus zwitterionic lipids (POPC), b) aggregation of vesicles, and above a certain concentration threshold to c) integration of the peptide into the bilayer and finally d) to the disruption of the bilayer structure. The understanding of the mechanism of action of this peptide in relation to the properties of its constituent amino acids is a first step in designing better peptides in the future.

1. Introduction

Antimicrobial peptides are important components of innate immune defense against a variety of microbial infections. They directly target and permeate bacterial membranes eventually leading to bacterial death. Due to the relative invariant nature of the bacterial membrane components and its importance in protecting the microbe, antimicrobial peptides which specifically target the bacterial membrane have been considered promising drug candidates, as a substitute or addition to conventional antibiotics to which many pathogens have acquired resistance [1–5].

Naturally occurring antimicrobial peptides are widely distributed in host organisms including plants, insects, amphibians and mammals [6–9]. Until now, more than 800 antimicrobial peptides have been identified in eukaryotes (http://www.bbcm.units.it/~tossi/amsdb.html, Antimicrobial Sequences Database). Many antimicrobial peptides display a broad spectrum of antimicrobial activity against pathogens. For example, magainins show antimicrobial activity against gram-positive bacteria, gram-negative bacteria, fungi, protozoa and some viruses [10–12]. Gramicidin S has considerable antimicrobial activity against gram-positive bacteria, gram-negative bacteria and several fungi in liquid media [13,14]. However, a number of antimicrobial peptides are also cytotoxic to mammalian cells, which limits the direct use of these peptides as therapeutics. As a result, great efforts are being made to modify the native antimicrobial peptides or design new synthetic peptides to achieve better specificity against microbial infections with the lowest side-effect on the host organism. A variety of methods have been applied to design new antimicrobial peptides based on the characteristics of the native peptides, such as replacing some amino acid residues, changing the chirality of peptides, hybridizing different peptide segments to form new

Abbreviations: V4, cyclized CVKVQVKVGSGVKVQVKVC by an internal disulfide bond; TV4, VKVQVKVGSG; LPS, lipopolysaccharides; LB, Langmuir film balance; DPI, dual polarization interferometry; FCS, fluorescence correlation spectroscopy; REV, Rho 6G entrapping large unilamellar vesicle; RLV, Rho-PE labeled large unilamellar vesicle; GUV, giant unilamellar vesicle; POPC, 1-Palmitoyl-2-Oleoyl-sn-Glycero-3-Phosphocholine; POPG, 1-Palmitoyl-2-Oleoyl-sn-Glycero-3-[Phospho-rac-(1-glycerol)]; Rho-PE, 1,2–Dipalmitoyl-sn-Glycero-3-Phosphoethanolamine-N-(Lissamine Rhodamine B Sulfonyl) (Ammonium Salt); NBD-PE, 1,2-Dipalmitoyl-sn-Glycero-3-Phosphoethanolamine-N-(7-nitro-2-1,3-benzoxadiazol-4-yl) (Ammonium Salt); Cap Biotinyl-DPPE, 1,2-Dipalmitoyl-sn-Glycero-3-Phosphoethanolamine-N-(Cap Biotinyl) (Sodium Salt); MW, molecular weight

* Corresponding author.
E-mail address: chmwt@nus.edu.sg (T. Wohland).

0005-2736/$ – see front matter © 2008 Elsevier B.V. All rights reserved.
doi:10.1016/j.bbamem.2008.10.005

chimaeric peptides and *de novo* peptide designs [15–22]. Antimicrobial peptides are usually short in length, which opens the possibility of chemical peptide synthesis to realize the designed peptide.

Lipopolysaccharide (LPS), also known as endotoxin, is the major component on the outer leaflet of the outer membrane of gram-negative bacteria [23–26]. The study of endotoxin-binding host defense proteins showed that an endotoxin-binding motif which plays an important role in killing bacteria may be formed by amphipathic sequences rich in cationic residues [27]. Therefore those antimicrobial peptides which have strong ability to bind to endotoxin and disrupt membranes have attracted extensive interest for drug development. Frecer and colleagues made a *de novo* design of antimicrobial peptides based on some sequences of endotoxin-binding host defense proteins [28]. They designed a series of short symmetric amphipathic peptides containing endotoxin-binding sequence HBHPHBH and HBHBHBH (B: cationic residue; H: hydrophobic residue; P: polar residue) with a β-sheet conformation to determine whether introduction of the endotoxin binding motif could enhance the antimicrobial activities of cyclic cationic peptides. Amongst these peptides, one named V4 is prominent (cyclized CVKVQVKVGSGVKVQVKVC by the internal disulfide bond). V4 has a good combination of high antimicrobial activity, low cytotoxic activity and low hemolytic activity compared to other synthetic and native peptides. V4 demonstrated a specificity 2400-fold greater than that of Polymyxin B, which resulted from the higher level of antimicrobial activity and the lower level of hemolytic activity of the V4 peptide. Further study on the in vitro interaction between V4 and lipid membranes, including different lipid components, shows that besides the high binding affinity for LPS and lipid A (the bioactive part of LPS), V4 also displays a higher affinity for negatively charged phospholipids than for zwitterionic phospholipids. The strong binding of V4 to the negatively charged lipids showed that electrostatic force is a prerequisite for its selectivity on bacterial membranes, in contrast to mammalian cell membranes [29]. Recently, we have demonstrated in a comparison of several antimicrobial peptides that V4 can aggregate lipid vesicles and can lead to vesicle leakage [30]. However, a detailed explanation of its action has not been attempted.

In the present study we investigate the action of V4 in binding and disrupting membranes and compare its action to a truncated inactive version of V4, called TV4. Different lipid membrane models were used including lipid monolayers, solid supported bilayers and liposomes. We combine several techniques: Langmuir Blodgett (LB) film balance, atomic force microscopy (AFM), dual polarization interferometry (DPI), fluorescence correlation spectroscopy (FCS) and confocal imaging, to investigate the various steps of interaction between V4 and different membrane models. At the same time, negatively charged and zwitterionic phospholipids were used to examine the effect of electrostatic and hydrophobic interactions on the action of V4 on the membranes.

2. Materials and methods

2.1. Materials

Rhodamine 6G chloride (Rho 6G) and avidin are products from Molecular Probes (ITS Science and Medical Pte Ltd., Singapore). Triton-X100 and phosphate buffered saline (PBS, pH 7.4) were purchased from Sigma-Aldrich (Sigma-Aldrich Pte Ltd, Singapore). 1-Palmitoyl-2-Oleoyl-sn-Glycero-3-Phosphocholine (POPC), 1-Palmitoyl-2-Oleoyl-sn-Glycero-3-[Phospho-rac-(1-glycerol)] (POPG), 1,2-Dipalmitoyl-sn-Glycero-3-Phosphoethanolamine-N-(Lissamine Rhodamine B Sulfonyl) (Ammonium Salt) (Rho-PE), 1,2-Dipalmitoyl-sn-Glycero-3-Phosphoethanolamine-N-(7-nitro-2-1,3-benzoxadiazol-4-yl) (Ammonium Salt) (NBD-PE) and 1,2-Dipalmitoyl-sn-Glycero-3-Phosphoethanolamine-N-(Cap Biotinyl) (Sodium Salt) (Cap Biotinyl-DPPE) were purchased from Avanti (Avanti Polar Lipids, Inc., Alabaster, AL). V4 and V4-TMR which is the V4 labeled with dye tetramethylrhodamine (TMR) at the N-terminus were synthesized by Genemed (Genemed Synthesis, Inc., South San Francisco, CA). In addition, we used a truncated V4 (TV4: VKVQVKVGSG) as a control peptide (Genemed Synthesis). According to the HPLC data provided by the company, the purity of V4-TMR was about 84% and the purity of V4 was above 97%.

2.2. Interaction of V4 with lipid monolayers

2.2.1. Penetration study

The penetration study of V4 into monoloayers was performed on a Langmuir film balance (model 601 M, NIMA Technology Ltd. England). The required volume of POPG or POPC chloroform solution with a final lipid concentration of 0.2 mM was spread on the water surface in a drop-wise manner, making sure that the surface pressure did not change after lipid deposition. After solvent evaporation for 10 min, the monolayer was compressed to a target surface pressure. The lipid monolayer was allowed to adjust until a constant molecular area was achieved. Afterwards an appropriate volume of V4 solution (dissolved in water with high concentration) was injected underneath the monolayer into the subphase, generating different peptide concentrations in the trough. The surface pressure change (Δπ) with time at a fixed molecular area was recorded.

2.2.2. AFM study

A lipid/V4 mixed monolayer formed in the LB trough was transferred by a Langmuir Blodgett transfer to freshly cleaved mica. For this purpose a mica plate is vertically placed in the water subphase of the LB trough before lipid was spread on the water surface. After the penetration experiment, the surface pressure was kept constant at the surface pressure of complete penetration. The mica was slowly extracted from the subphase. The monolayer on the mica was dried in a desiccator overnight before AFM imaging.

AFM was performed in air on the NanoScope IIIa MultiMode Scanning Probe Microscope (Digital Instruments Inc., Santa Barbara, CA, USA). Topographic images were acquired in tapping mode. The typical scan rates ranged from 1 to 1.25 Hz depending on the scan size. The monolithic silicon probes (NanoWorld AG, Switzerland) with a cantilever length of 125 μm and force constant of 42 N/m were used for measurements. Images were obtained and analyzed by the Nanoscope software provided by the company. Images from at least two different samples prepared on different days with several macroscopically separated areas on each sample were acquired for data reproducibility.

2.2.3. Isotherm study

A Langmuir film balance was used for isotherm studies of V4 interacting with lipid monolayers. POPG and POPC were dissolved in chloroform with a concentration of 0.2 mM. Due to the low solubility of V4 in chloroform, V4 was first dissolved in the minimal volume of methanol to prepare a clear solution. Additional chloroform was then added to prepare a solution with a V4 concentration of 0.2 mM. The required volume of POPG or POPC was mixed with V4 to form lipid/V4 mixture with V4 percentage of 0%, 5%, 10%, 20%, 33%, 50% and 100%. An appropriate volume of individual lipid/V4 mixed solution was deposited on the water surface. The lipid monolayer formed spontaneously on the air-water interface in the absence or in the presence of V4. After solvent evaporation for 10 min, the monolayer was compressed and the isotherm was record. Each curve was repeated at least twice for reproducibility.

The stability of a monolayer is determined by the excess Helmholtz energy according to the method developed by Zhao and Feng [31,32]. The excess Helmholtz energy (ΔA_m^{ex}) was defined as the deviation from

the ideal value of the Helmholtz energy according to the following equation.

$$\Delta A_m^{ex} = \int_{A_0}^{A} [\pi_{12} - (X_1\pi_1 + X_2\pi_2)]dA$$

A_0 and A are the molecular area where the surface pressure begins to increase from zero and where the Helmholtz excess energy is calculated, respectively. π_{12}, π_1 and π_2 are the surface pressure of mixed monolayer, pure lipid monolayer and pure V4 monolayer at the molecular area of A, respectively. X_1 and X_2 imply the percentage of lipid and V4 respectively in the mixed monolayer.

2.3. Interaction of V4 with solid supported bilayer

2.3.1. Small unilamellar vesicles (SUVs) preparation

Lipids were prepared as stock solutions in chloroform. The solvent was evaporated under N_2 gas and then the samples were placed into vacuum for at least 1 h. PBS buffer was added to re-dissolve the lipids to give an aqueous suspension with a concentration of 0.5 mM. SUVs were prepared by freeze — thawing the lipid suspension 5 times followed by extrusion through 0.05 μm polycarbonate membrane filters 20 times using a mini-extruder syringe device (Avanti Polar Lipids).

2.3.2. Insertion of V4 into solid supported bilayer as analysed by DPI

Dual polarization interferometry (DPI) was used to investigate the interaction of V4 and TV4 with solid supported bilayers (POPG and POPC). DPI is a surface based technique making use of functionalized glass waveguides integrated into a flow cell. Illuminating the stack of waveguides produces an interference pattern which changes according to the material deposited on the upper waveguide, allowing the determination of opto-geometrical properties (mass, density and thickness) of adsorbed layers at a solid-liquid interface [33–35].

Common optical biosensing techniques such as Surface Plasma Resonance make use of singly polarized light to produce an evanescent field close to the solid liquid interface, and consequently thickness (d) and refractive index (n) of material added at the solid liquid interface cannot be measured independently. By contrast DPI uses two different polarizations of light, termed Transverse Magnetic (TM) and Transverse Electronic (TE), allowing the dimensions of an adsorbed isotropic layer at the waveguide surface to be calculated using a convergence algorithm fitted to the measured phase changes from the two polarizations [33,36].

In certain circumstances a surface layer will be formed from uniaxial molecules where the polarisability along the length of the molecule is different from across the molecule, such as liquid crystals. Where these molecules are aligned with respect to the surface the net angle of alignment will determine the extent to which the refractive index of the layer is different if measured parallel or perpendicular to the surface. Such an optically anisotropic overlayer will introduce an additional unknown through the difference in the refractive index of the layer as measured by the 2 polarizations TM and TE. In other words, for an isotropic layer the refractive index of the layer as measured by TM is the same as measured by TE, $n_{TM} = n_{TE}$, but for an anisotropic layer $n_{TM} \neq n_{TE}$. Failing to take account of the anisotropy of the layer will result in the mis-reporting of measured opto-geometric parameters, and will affect all optical techniques [37].

To analyze such an anisotropic layer one of the three parameters, thickness (d), refractive index (n) or the difference in layer RI, as measured by TM as compared to TE (n_{TM}–n_{TE}) is fixed and the other two determined from the measured changes in phase from the 2 polarizations.

A prime example of an anisotropic layer is a lipid bilayer, where the alignment of lipids orthogonal to the solid substrate increases the refractive index of the lipids as measured by TM compared to TE. The assumption of an isotropic refractive index for the lipid layer would lead to an over estimation of lipid layer thickness and mass.

The data presented here is obtained by fixing the thickness of the lipid bilayer to be 4.0 nm, as determined by neutron scattering [38]. Assuming that this thickness is correct the obtained difference n_{TM},–n_{TE} will closely correspond to the birefringence of the overlayer.

A more strict definition of birefringence is the difference in refractive index of the layer perpendicular (n_e) and parallel (n_o) to the surface. For the purposes described here it is sufficient to describe birefringence in terms of n_{TM}-n_{TE} [39].

In an example where a lipid layer moved from a less ordered to more ordered (aligned) state the difference in refractive index of the layer as measured by TM and TE would increase and thus so would the reported birefringence. In the case where the alignment of the lipid chains was disrupted, for example by an antimicrobial peptide inserting into the lipid chains, the measured birefringence would decrease. A peptide associating with the surface of a lipid layer, but not inserting into the lipid layer would not be expected to significantly alter the measured birefringence of the layer.

To form lipid bilayers, liposomes were flowed onto the glass waveguide surface where the SUVs were allowed to deform and fuse to form lipid bilayers [40]. Following establishment of stable layers various concentrations of V4 and on a separate bilayer various concentrations of TV4 were then flowed over the bilayers with mass and structural changes to the bilayer recorded.

2.4. FCS study of V4 and TV4 interacting with POPG REVs

FCS was used to investigate membrane permeation by V4 and TV4. The preparation of POPG or POPC REVs and RLVs was described previously [29,30,52]. The stock solution of POPG REVs was diluted and mixed with different concentrations of V4 and TV4. The final lipid concentration was 40 μM. V4 concentrations were 1, 2, 5, 10, 15 and 20 μM with corresponding peptide:lipid ratio of 1:40, 1:20, 1:8, 1:4, 1:2.67 and 1:2. The concentrations of TV4 were 2, 20, 200 and 2000 μM. As control, 0.05% triton-X100 was also added to completely disrupt REVs. FCS experiments were performed after 1 h incubation at room temperature. The FCS instrument includes a Zeiss Axiovert 200 inverted microscope, an Argon-Krypton laser with a 515 nm line, matching dichroic filter and emitter, highly sensitive avalanche photodiodes (APD) detector. A dichroic filter (525DRLP) and an emitter (545AF35) for REVs were used to separate the excitation light from the emission fluorescence.

Fluorescence correlation spectroscopy is a technique with single molecule sensitivity [41]. It analyzes the fluorescence intensity fluctuation within a tiny confocal volume due to the minute deviations from thermal equilibrium. The detailed theory can be found in literature[42–50]. For 3D diffusion processes, the measured fluorescence photon count rates autocorrelation function (ACF) $G(\tau)$ can be fitted as follows:

$$G(\tau) = \frac{1}{N}\frac{\sum_{i=1}^{n}\left(\frac{Q_i}{Q_1}\right)^2 F_i\left(1+\frac{\tau}{\tau_{Di}}\right)^{-1}\left(1+\frac{\tau}{\left(\frac{z}{\omega}\right)^2\tau_{Di}}\right)^{-1/2}}{\left[\sum_{i=1}^{n}\frac{Q_i}{Q_1}F_i\right]^2} + G_\infty$$

N is the average number of particles in the confocal volume. Q_i is the fluorescence yield of particle i. The coefficients F_i are the mole fraction of species i in the sample. τ_{Di} is the lateral diffusion time of the fluorescent particle staying in the confocal volume. ω and z are the radial and axial distances of the confocal volume at which the intensity has dropped by $1/e^2$ of the maximum value. G_∞ is the convergence value of the ACF for long times, in general this value is 1. The program IgorPro (Wavemetrics, Lake Oswego, OR, USA) was used to fit the autocorrelation function to the experimental data as

described previously [49]. Diffusion time τ_{Di} and particle number in the confocal volume N are the two main parameters provided by FCS for analysis. In a system with more than one fluorescent species, diffusion time, particle number in the confocal volume, and mole fraction of each fluorescent species can be distinguished by FCS.

2.5. Interaction of V4 with giant unilamellar vesicles (GUVs)

2.5.1. GUVs preparation

The POPG or POPC solution (5 mg/mL) was mixed with 3 mol% of Cap Biotinyl-DPPE and 0.5% NBD-PE in chloroform. After evaporating the sample by a rotary evaporator for 2 h, 2 mL water was added to achieve a suspension of phospholipid with final lipid concentration of 500 μM. This solution was incubated at 40 °C for 12 h. The lipid GUVs formed spontaneously.

2.5.2. Immobilization of GUVs on coverslip

An avidin solution (0.5 mg/mL) was deposited on a cleaned coverslip. After incubation for 15 min and air drying, lipid GUVs were deposited on the avidin coated coverslip. The interaction between avidin and biotin lead to the immobilization of GUVs on the coverslip.

2.5.3. Confocal imaging

In these experiments the fluorescently labeled V4-TMR is used. The labeling has limited influence on the antimicrobial activity of the peptide, and V4-TMR shows similar properties as V4 and leads to vesicle leakage at the same concentrations (data not shown). A GUVs solution (250 μM) was first premixed with V4-TMR (0.5 μM) to achieve a more homogenous distribution of V4-TMR on GUVs. After depositing this mixture on the coverslip, unlabeled V4 was added and confocal images were taken. Confocal imaging was performed on a Fluo-ViewTM FV300 system with an Argon laser (488 nm) and HeNe laser (543 nm) exciting NBD-PE and V4-TMR, respectively.

3. Results

3.1. Penetration of V4 into POPG and POPC monolayers

Lipid monolayers on the LB trough were compressed to a target surface pressure of 15 mN/m. For measurements of peptide action on the lipids, the monolayer was kept at a constant surface area. The injection of peptide into the subphase of the lipid monolayer induces a surface pressure change, which indicates the binding or insertion of the peptide into the lipid monolayer. Fig. 1 shows the surface pressure increase (Δπ) induced by the interaction between V4 and POPG and POPC monolayers. With the increase in V4 concentration, an increase in surface pressure is observed until a peptide concentration of 0.5 to 1.0 μM at which the interaction reached saturation. Further addition of V4 did not result in any further increases of Δπ. V4 induced a higher surface pressure increase Δπ on the negatively charged POPG monolayers compared to the zwitterionic POPC monolayers at all concentrations.

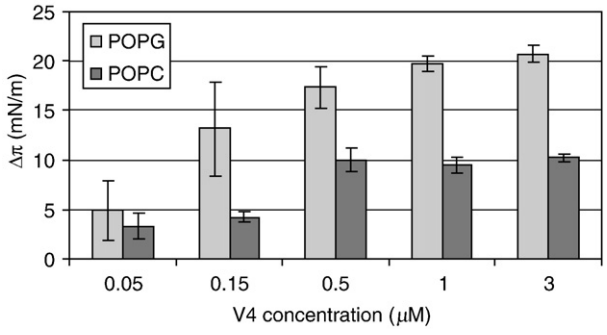

Fig. 1. Langmuir–Blodgett trough experiments. The graph shows the surface pressure increase (Δπ) induced by the interaction between V4 and POPG and POPC monolayers on a Langmuir film balance as a function of V4 concentration. At each peptide concentration, V4 shows stronger affinity for POPG than for POPC.

3.2. AFM study of V4 penetrating into POPG and POPC monolayers

POPG and POPC monolayers in the absence or presence of V4 were transferred onto mica and AFM was performed to investigate the effect of V4 on the morphology of the monolayers. The morphology of pure POPG and POPC monolayers at the surface pressure of 15 mN/m is shown in Fig. 2A and C. In the absence of peptide, the AFM images displayed a regular and flat area for both lipids, which indicated that lipid molecules formed a homogenous monolayer. The section analysis of POPG and POPC monolayers provides the cross-section profile of the monolayers with regard to height difference. It can be observed that the height difference of the pure lipid monolayer was 0.29 and 0.23 nm for POPG and POPC, respectively. An increase of surface pressure up to 30 mN/m did not affect the morphology of the pure monolayers which stayed flat with a height difference of 0.40 nm (data not shown).

Fig. 2B and D show the AFM images of monolayers of V4 with POPG and POPC, respectively. At peptide concentration of 50 nM, some thin and long filaments which were randomly distributed protruding over the monolayer surface were observed shown as bright regions. The filaments illustrated in the figure were up to about 200 nm in length and 10 nm in width. These protrusions were probably aggregates of V4 possibly in combination with lipids, which penetrated the monolayer, strongly interacted with lipid molecules and accumulated on the hydrophobic part of the POPG and POPC monolayers. The section analysis of POPG and POPC monolayers with V4 penetration shows that the height difference of the two arrows indicated on the two AFM images is 1.53 and 0.94 nm, respectively. Besides the long filaments, some small holes indicated by dark spots were also observed on the POPG monolayer but not on the POPC monolayer. This confirmed the strong interaction between V4 and POPG, probably removing some lipid molecules from the POPG monolayer. Fibril formation could also be observed at concentrations of 500 nM and a surface pressure of 32 mN/m (data not shown). The three height levels detected on POPG layers correspond to defects in the layers, the monolayer surface and the fibrils on accumulated on the hydrophobic part of the monolayer. The formation of the filament structure upon interaction of V4 with lipid monolayers is similar to previous accounts in literature. Plenat et al. reported that some cell penetrating peptides form fibrils with and without lipids, self-associate and form supermolecular complexes to perform their function [55].

3.3. Isotherm study of lipid/V4 monolayers

During compression isotherms of pure POPG and POPC began to rise at a molecular area of 107 Å and 96 Å, respectively. With increasing compression, the surface pressure increases continuously until the collapse pressure of 45.8 ± 0.3 mN/m and 44.5 ±0.8 mN/m for POPG and POPC, respectively. Both lipids, which have the same hydrophobic tail groups and differ only in their hydrophilic head groups, showed similar isotherms.

Pure V4 showed strong surface activity compared with the lipids. At a molecular area of 125 Å, the isotherm of V4 began to rise. With increasing compression, the surface pressure of V4 monolayer continuously increased to 44.1 ± 1.9 mN/m, which was comparable to the collapse pressure of POPG and POPC.

The isotherms of pre-mixed POPG/V4 and POPC/V4 monolayers shifted right to higher molecular areas with increasing percentage of V4. The surface pressure (π) and molecular area (A) isotherms of premixed POPG/V4 and POPC/V4 are shown in Fig. 3. The collapse pressure for all isotherms was similar except for the POPG/V4 mixture with 50% V4 incorporation, which was an incomplete isotherm

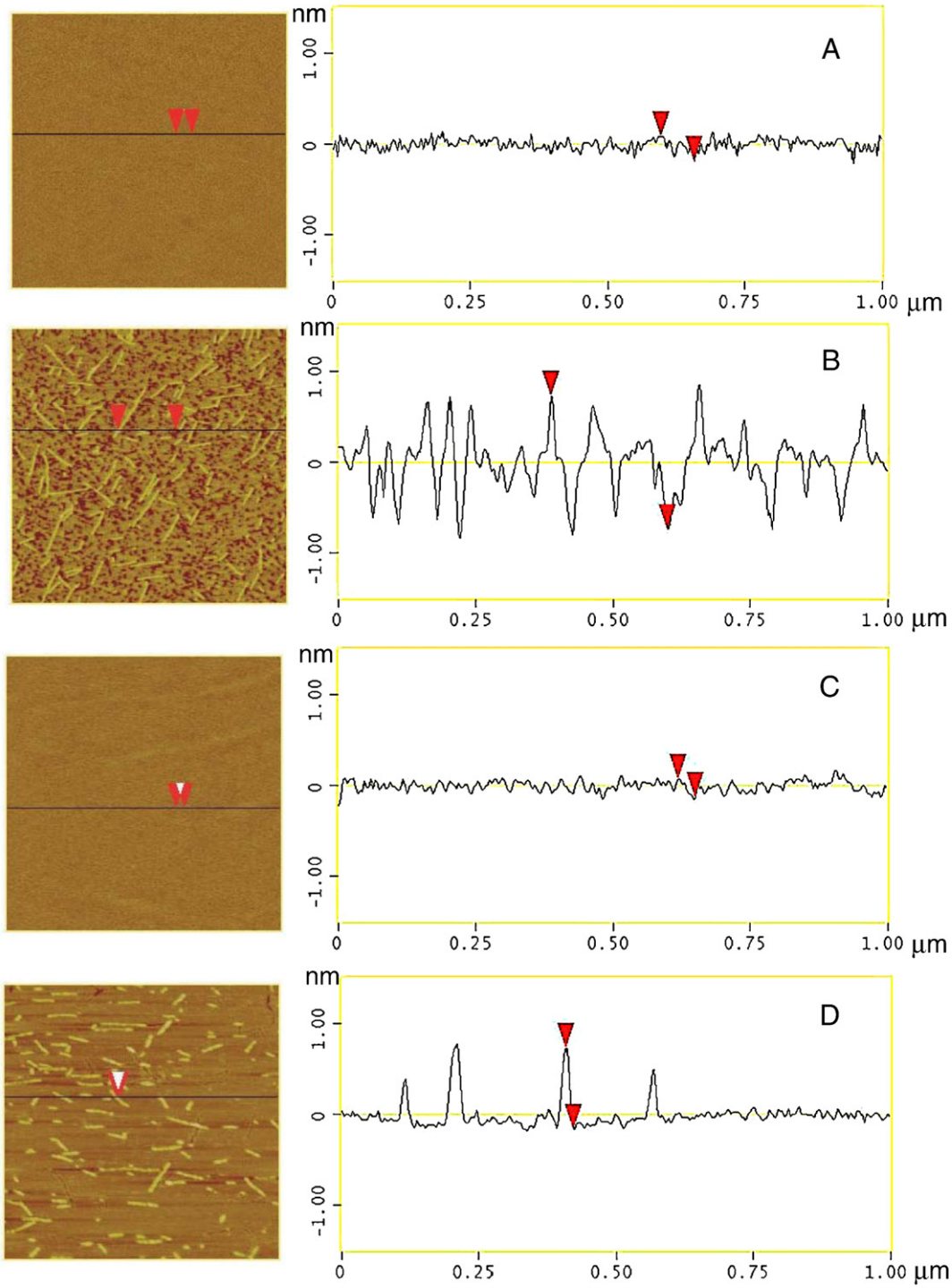

Fig. 2. (A) Left: AFM topographic images of pure POPG monolayer. Right: Section analysis of pure POPG. The height difference indicated by the two arrows is 0.29 nm. (B) Left: AFM topographic images of POPG monolayer penetrated by 50 nM V4. Right: Section analysis of POPG/V4 monolayer. The height difference indicated by the two arrows is 1.53 nm. (C) Left: AFM topographic images of pure POPC monolayer. Right: Section analysis of pure POPC. The height difference indicated by the two arrows is 0.23 nm. (D) Left: AFM topographic images of POPC monolayer penetrated by 50 nM V4. Right: Section analysis of POPC/V4 monolayer. The height difference indicated by the two arrows is 0.94 nm.

because the two barriers were too close and collapse was not observed. Comparing all the molecular areas at which the surface pressure began to increase (lift-off area), it is found that with increasing incorporation of V4, the lift-off areas gradually increase for both lipids, which indicates that V4 has an area-expanding effect on the lipid monolayer at low surface pressure. It should be noted, that the POPG/V4 mixtures of 20% and above reproducibly show a characteristic kink in the isotherms indicating a change in the monolayer properties at these concentrations.

Fig. 4 shows the excess Helmholtz energy change at different molecular areas. For both POPG and POPC, the presence of V4 in the mixed monolayer induced a negative deviation from ideal mixing. The negative excess Helmholtz energy indicated that there is interaction between lipid and V4, resulting in a lower energy of the stable system [31,32]. With increasing percentage of V4 from 0 to 50%, the excess Helmholtz energy continuously decreased, which indicates an increasing interaction between lipid and V4 and a gradual increase in system stability. The minimal excess energy, which corresponded to the most

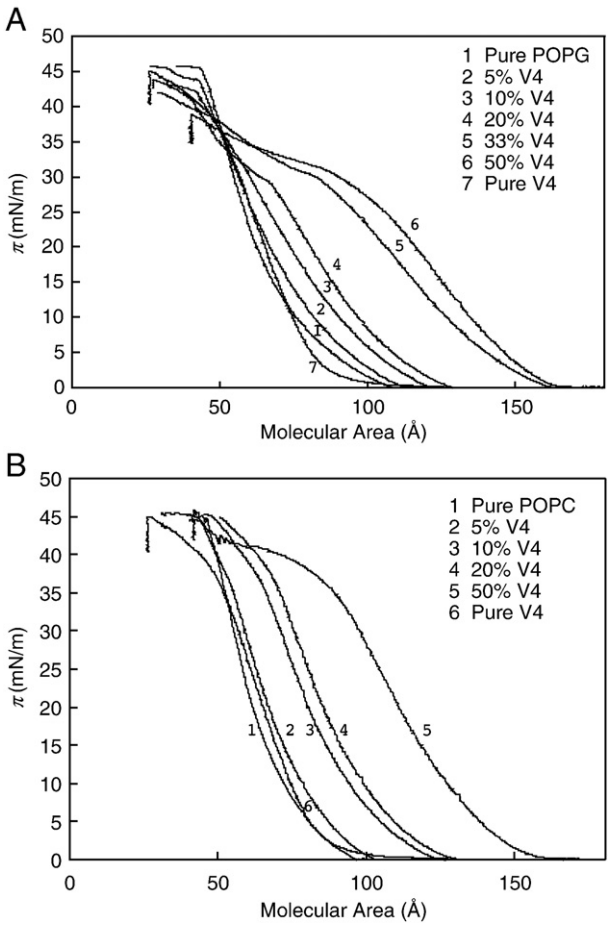

Fig. 3. Isotherms of mixed POPG/V4 and POPC/V4 monolayers recorded on a Langmuir–Blodgett trough with V4 percentage of 0%, 5%, 10%, 20%, 50% and 100% (corresponding peptide/lipid ratio of pure lipid, 1:19, 1:9, 1:4, 1:1 and pure peptide).

stable system within the studied V4 incorporation, was obtained in the presence of 50% V4 in the mixed monolayer. When V4 was incorporated into the monolayer with the percentage from 0% to 50%, V4 increased the system stability. The comparison of pre-mixed POPG/V4 and POPC/V4 monolayers shows comparable excess Helmholtz energies at 50% V4 incorporation. However at 10% and 20% V4 incorporation, V4 induced a larger energy decrease for POPC than for POPG.

3.4. Interaction of V4 and TV4 with solid supported bilayers

Biological cell membranes are composed of lipid bilayers and consequently one expects solid supported bilayers to more closely resemble cell membranes compared to monolayers at an air-water interface. Therefore the interaction of V4 with solid supported bilayers was investigated by DPI to explore the action of these peptides on model membranes. The deposition of POPG and V4 were followed on separate amine modified sensor chip surfaces. A 10 μM V4 solution, corresponding to the maximum concentration used in these experiments was injected into the sample chamber on a clean amine modified sensor chip. Near zero non-specific binding was observed and the surface coverage was measured at 0.054 ng/mm^2. Compared to V4, the addition of POPG SUVs to the amine surface led to high surface coverage, with typical, coverage values >2.6 ng/mm^2.

3.5. Stoichiometry of lipid: peptide interaction

Using a refractive index increment (RII) for lipid of 0.135 g/cm^3 [51], the POPG layer (that was to be challenged with V4) had a mass of 2.65 ng/mm^2 or 3.437×10^{-12} moles/mm^2. Using an RII of 0.184 g/cm^3 for protein, the mass of V4 that bound to POPG during the first (4 μM) injection was 0.069 ng/mm^2, which taking MW of V4 as 2027 is 3.40×10^{-14} moles, giving a POPG:V4 stoichiometry of 101:1. Taking the total mass of V4 bound over all the injections (0.414 ng/mm^2) a stoichiometry of 16.8:1 was obtained for POPG:V4.

For the POPG layer challenged with TV4 the measurements yielded a mass of 2.74×10^{-9} g/mm^2 or 3.55×10^{-12} moles/mm^2. Mass of bound TV4 during first injection was 0.02×10^{-9} ng/mm^2 and using a MW of 1042 for TV4 gives 1.92×10^{-14} moles and a POPG:TV4 stoichiometry of 185:1. Total mass of TV4 bound was 0.077 ng/mm^2 and thus a stoichiometry of 48:1.

3.6. Comparison of the mass and birefringence (alignment) changes induced by V4 and TV4.

The dual polarization instrument has a dual fluidic system enabling a side by side comparison of the action of sample and control. The data in Fig. 5A shows that at all added concentrations of V4 the mass of V4 binding to POPG was significantly greater than to the control POPC layer. This is especially evident at the higher concentrations of V4. The data also suggests the electrostatic attraction of a PC bilayer is lower than for PG. The binding of V4 at 10 μM to PC is 19% of that compared to PG.

Fig. 5B shows the changes in mass and in the birefringence, i.e. alignment within the lipid layer, during V4 and TV4 addition to POPG. Addition of TV4 to the POPG bilayer showed no change in birefringence strongly suggesting TV4 did not induce any change in the alignment of the lipid tails. In contrast the addition of V4 showed a significant decrease in the birefringence of the POPG layer with each injection of V4, indicating there is significant disruption to the alignment of the lipid chains induced by the insertion of the hydrophobic chains of V4.

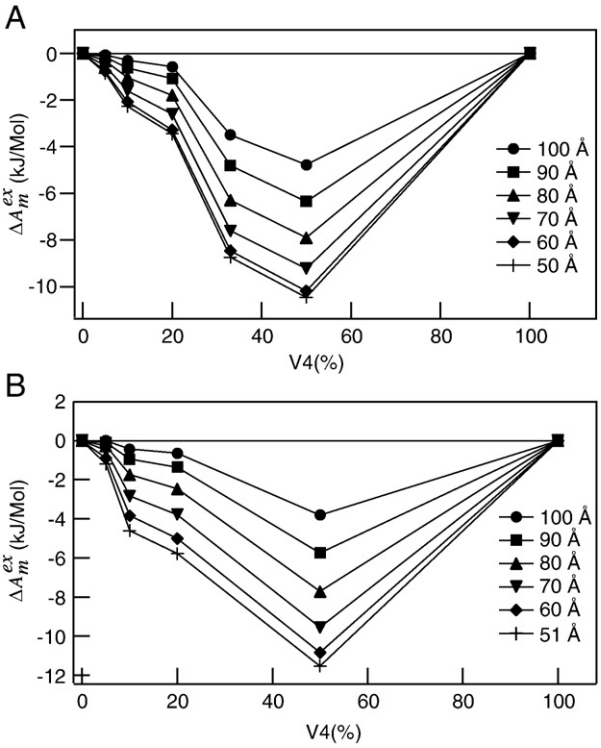

Fig. 4. Excess Helmholtz energy of POPG and POPC monolayers incorporated with different percentage of V4. (A) POPG; (B) POPC.

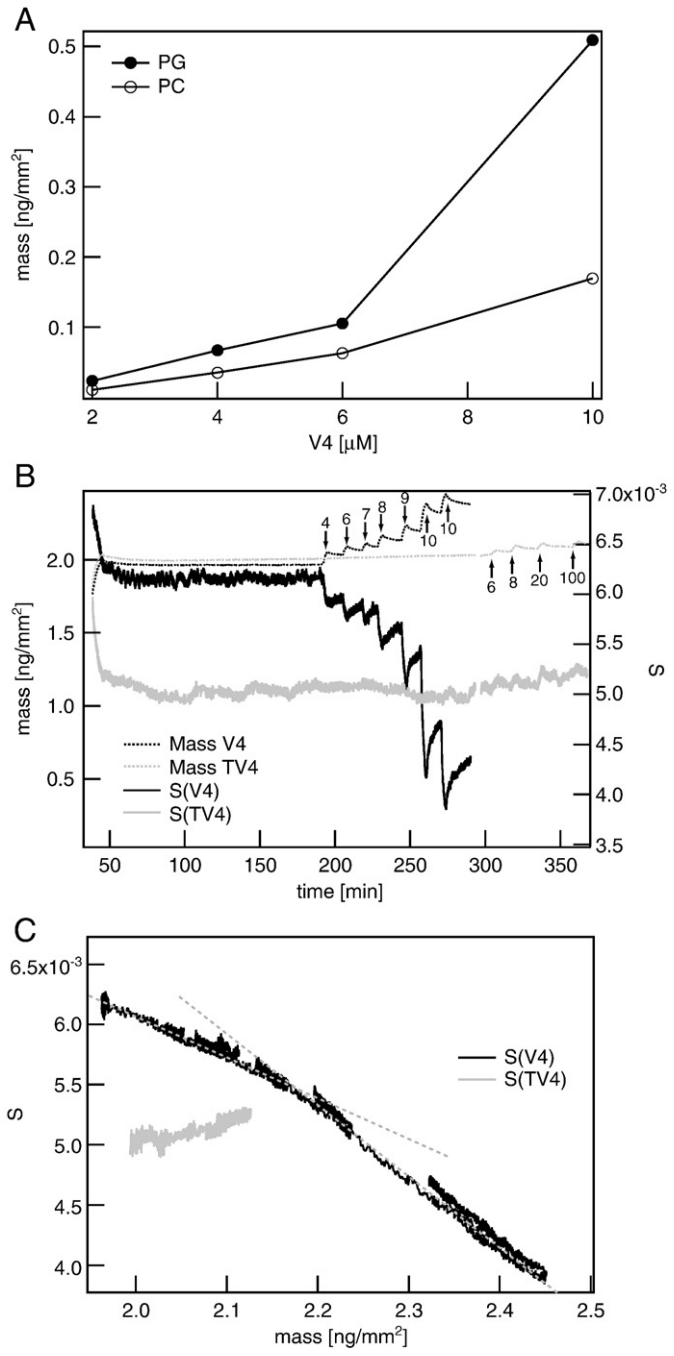

Fig. 5. Dual polarization interferometry (DPI) experiments. (A) Change of mass versus V4 concentration as injected on a POPG or POPC bilayer. The data shows that V4 binding to POPG was greater than to the control POPC layer. (B) Mass and birefringence changes when V4 or TV4 are added to POPG bilayers. The numbers in the graph indicate the concentration in μM of V4 or TV4 added at different injections. (C) Change in birefringence against mass of peptide for V4 and TV4. At a mass of about 2.2 ng/mm^2 the rate of change in birefringence increases for V4 indicating changes in alignment within the lipid layer. The dashed lines are guides for the eyes.

Plotting the change in birefringence against mass of peptide bound emphasizes the two stage process V4 undertakes on interacting with POPG (Fig. 5C). The first stage can be thought of as V4 accumulating on the surface of POPG, whilst the second stage (>2.2 ng/mm^2) correlates with insertion across the whole bilayer. In other words there is a threshold amount of V4 that must accumulate before significant insertion, (as evidenced by an increase in the rate of birefringence change) is observed to take place.

3.7. Membrane permeation and disruption

In a previous report we have given detailed information about fluorescence correlation spectroscopy (FCS) measurements of the interaction of V4 with two different membrane models [30]. REVs and rhodamine-PE labeled vesicles (RLVs) have been used to determine whether V4 leads to membrane permeation, i.e. fluorophore leakage from REVs, and whether the permeation originates from pore formation or membrane disruption, i.e. whether RLVs are kept intact during vesicle leakage. Results clearly indicated that V4 leads to POPG vesicle leakage by a membrane disruptive process (at a V4:lipid ratio of 1:2), in contrast to pore formation, and that before vesicle disruption a step of vesicle aggregation can be detected at a V4:lipid ratio of 1:2.67. On POPC vesicles V4 did not show any changes up to V4:lipid ratios of 7.5:1. The ability of TV4, a control peptide, to induce membrane permeation and disruption was investigated here by fluorescence correlation spectroscopy. REVs were applied in this study to examine the effect of TV4 on the integrity of membranes [52]. For the REVs, if the peptide induced membrane permeation, Rho 6G, which was initially entrapped in the vesicles, will be released into the solution, resulting in an increased number of Rho 6G detected. The number of REVs, which are more fluorescent, will decrease, as well as its fraction. Simultaneously, due to the release of fluorescent dyes, the diffusion time of the

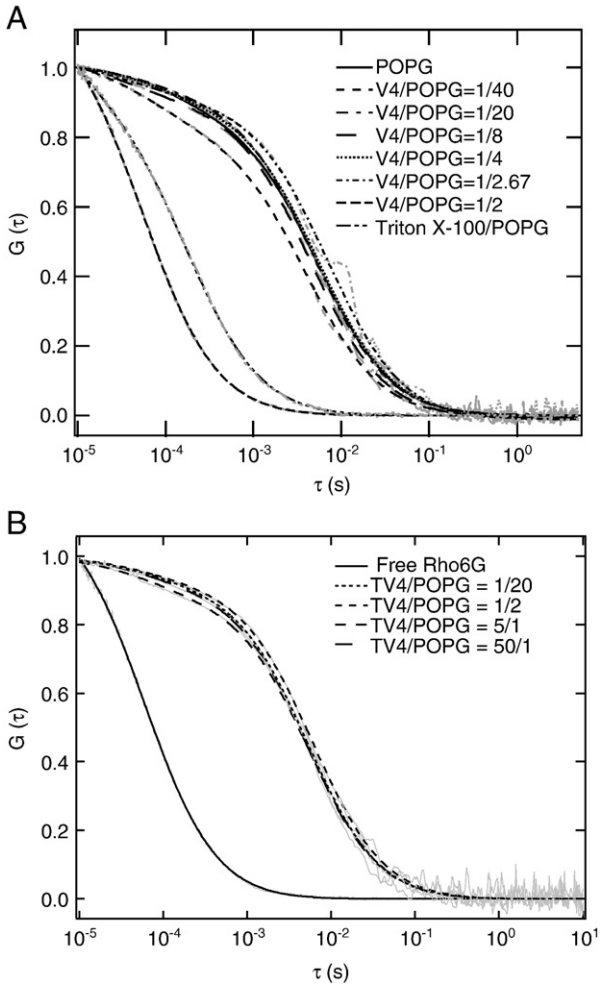

Fig. 6. Normalized ACFs of peptides interacting with POPG REVs recorded at different peptide:lipid ratios. The width of the ACF is an indicator for leakage. (A) V4 measurements: only at a concentration of V4:POPG=1:2 can leakage be observed. After experiments Triton ×100 is added to disrupt the vesicles. (B) TV4 measurements: even at peptide lipid ratios as high as 50:1, no leakage is observed.

fluorescent species τ_D will decrease. Therefore the change in particle number in the confocal volume N, contributed by both Rho 6G particle number (N_{rho}) and POPG REVs ($N_{vesicle}$), together with the diffusion time τ_D of the fluorescent particle provides information about membrane permeation or membrane disruption. In Fig. 6 we show the results of TV4 measurements and show for comparison previous results obtained with V4. In our previous study, V4 leads to dye leakage from POPG LUVs at a V4:lipid ratio of 1:2. As control we used TV4 with the same REV solution (Fig. 6B). Despite working at peptide:lipid ratios of up to 50:1, no decrease in correlation time could be detected and vesicles stayed intact.

3.8. Interaction of V4 with POPG and POPC GUVs

The GUVs were labeled with NBD-PE and were visualized with the 488 nm line of the confocal microscope. By contrast V4-TMR is excited by the 543 nm line. This double labeling strategy allows the differentiation of lipid bilayers with and without V4 attached. Fig. 7A shows a POPC GUV with a second vesicle inside. The image at 488 nm (A) shows both vesicles clearly due to the NBD-PE labeling. The image at 543 nm (B) shows only the outer membrane due to V4-TMR binding but no V4-TMR was detected in the inside of the GUV. When unlabeled V4 (up to 25 μM) was added to this mixture, V4-TMR was replaced and was removed from the POPC GUVs without compromising the integrity of the vesicles. The replacement of V4-TMR on the vesicle surface by the unlabeled V4 was proven by Fig. 8, which showed a decrease in both photon count rates and particle numbers on the POPC vesicle surface. In contrast, V4 acted differently on POPG GUVs (Fig. 7C–E). Firstly, due to the strong interaction between POPG GUVs and V4-TMR, the exchange of peptide between membrane and surrounding buffer is slow, which result in the inhomogeneous distribution of V4-TMR on

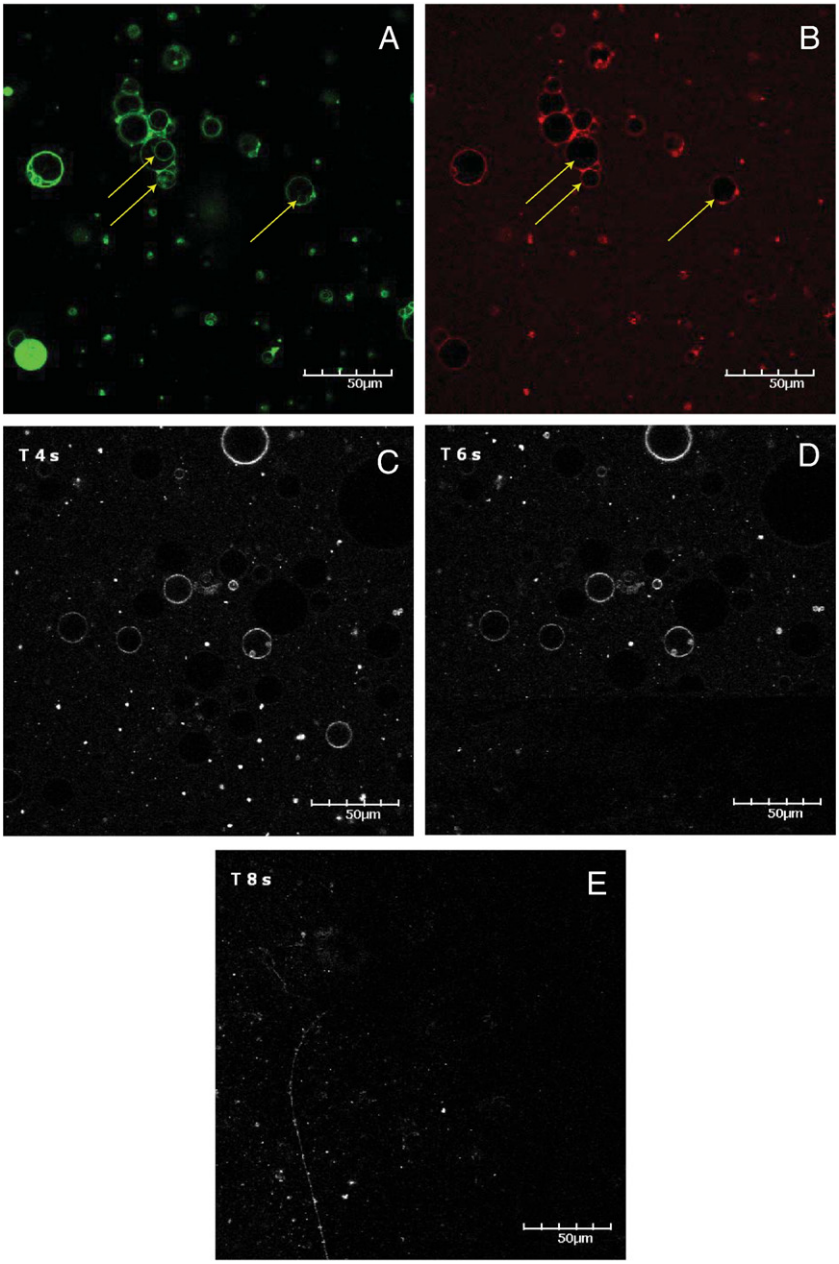

Fig. 7. Confocal images of V4 interacting with premixed POPC/V4-TMR and POPG/V4-TMR GUVs. (A) and (B) show the interaction between V4 and premixed NBD-PE labeled POPC/V4-TMR GUVs, excited by 488 nm and 543 nm laser, respectively. V4-TMR bound to the POPC GUVs surface. (C) to (E) illustrate the process of V4 disrupting premixed POPG/V4-TMR GUVs. (C) was taken 2 s before V4 addition. (D) is the moment of V4 adding on GUVs. (E) was taken 2 s after V4 addition.

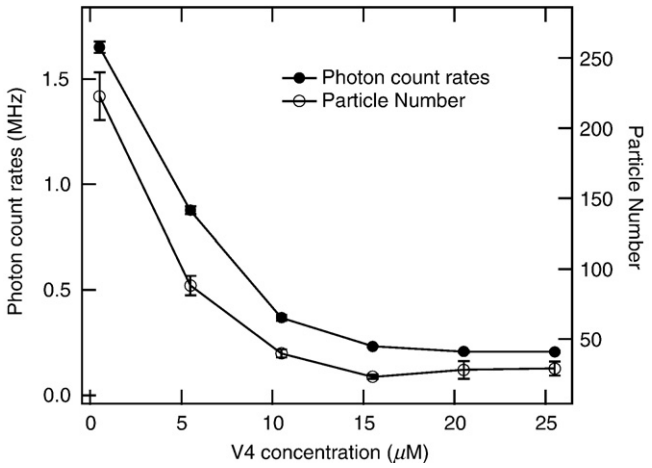

Fig. 8. Interaction of V4 with premixed POPC/V4-TMR GUVs. The decrease in both photon count rates and particle number in the confocal volume indicate the exchange between V4 and V4-TMR on the membrane surface.

different GUVs (Fig. 7C). Secondly, Upon V4 addition (5 μM one drop) to POPG GUVs, V4 rapidly induced membrane disruption within 2 s, which is in agreement with our previous FCS study on LUVs [29].

4. Discussion

4.1. V4 action mechanism

Based on the combination of experiments on V4-membrane interactions, we propose a possible action mechanism for V4. On a molecular level V4 first binds to the membrane surface due to electrostatic interactions. It is the cationic character of the peptide and thus the electrostatic forces which provide membrane selectivity and the affinity to allow peptide accumulation on the membrane. This is shown by the lack of exchange of labeled against unlabeled peptide on anionic lipid membranes and the binding studies in this work by LB, DPI and FCS experiments. V4 caused obvious exchange with V4-TMR on the POPC GUVs surface without entering the vesicle, indicating that V4 first binds to the membrane surface. This binding is a dynamic equilibrium. LB experiments also showed that with increasing V4 concentration, the surface pressure gradually increased, caused by the absorption of V4 on the monolayer surface. DPI experiments showed that V4 strongly binds to solid supported lipid bilayers, indicating that V4 has strong absorbing ability on the membrane. This process is mainly driven by electrostatic interaction. However, electrostatic interactions are not sufficient for membrane permeation as is seen by experiments with the truncated control peptide TV4, containing only one LPS binding motif (-VKVQVKV-), which binds to POPG but lacks the ability to integrate and disrupt POPG membranes. After absorption on the membrane surface, V4 oligomerizes or aggregates and inserts into the membrane, driven mainly by hydrophobic interactions. This interpretation is supported by the increase in the rate of change of birefringence in DPI experiments after a threshold concentration of V4 (~2.2 ng/mm^2) is reached. Further evidence of this might come from characteristic changes in the Langmuir isotherms observed at POPG/V4 mixtures with V4 concentrations of 20% and above. At these V4 concentrations characteristic kinks were observed in the isotherms indicating changes within the membrane. In addition, the continued change in birefringence suggests that the peptide changes the membrane structure probably due to insertion and translocation, and finally leads to membrane disruption. Furthermore, circular dichroism spectra of V4 in the presence and absence of POPG did not show any structural changes (unpublished results), excluding peptide folding as a mechanism for membrane insertion. This supports the hypothesis that aggregation or oligomerization is a necessary step for antimicrobial activity for V4. AFM experiments also showed that V4 caused some thin and long filaments protruding over the lipid monolayer surface. These filaments have the size of up to about 200 nm long, probably due to the V4 aggregates interacting with lipid. It should be noted that pure POPG monolayers did not change structure at higher surface pressures of ~30 mN/m and that fibril formation could be detected at the tested surface pressures from 15–30 mN/m. This indicates that the fibril formation is not a result of changes in lipid layer morphology due to surface pressure changes. Because AFM scanned the hydrophobic chain part of the lipid monolayer, the observation of the filaments indicated that V4 or V4 aggregates insert into the membrane, contact the hydrophobic chain of the lipid and undergo translocation. After the translocation, V4 disrupts the membrane at a V4:lipid ratio of 1:2. Finally this step causes bacterial death. We have shown previously, that V4 will aggregate vesicles in solution before disruption and vesicle leakage [30]. This is probably due to the high hydrophobicity of V4. At a high peptide:lipid ratio, a large number of V4 which is cationic neutralizes the negative charges of the vesicles, leading to a reduced electrostatic repulsion. The hydrophobicity of V4 brings the vesicles together to induce vesicle aggregation. However, as demonstrated by the confocal experiments on immobilized GUVs, this is not an essential step and membranes of immobilized vesicles will be disrupted in the absence of vesicle aggregation. The process of V4 induced membrane permeation and disruption is illustrated in Fig. 9. Firstly, V4 binds to or absorbs on the membrane surface. Secondly, some of V4 insert into the membrane and form peptide aggregates. After insertion, V4 traverses from the membrane surface to the inner layer of the membrane and induce membrane aggregation. Finally V4 disrupts the membrane, leading to bacterial death. However, it is also possible that peptide translocation and membrane aggregation happen simultaneously.

4.2. Effect of electrostatic interaction

Electrostatic forces play a significant role in V4-membrane interaction. The positive charges of V4 (4 lysines), similar to many antimicrobial peptides, facilitate the electrostatic interaction with the head groups of lipids consisting of negative charges and allow the peptide to accumulate on the membrane even at low solution concentrations. In contrast the reduced interaction with zwitterionic POPC vesicles does not allow a sufficient accumulation of the peptide on the membrane to induce any further effects. LB experiments, FCS measurements, DPI measurements and confocal imaging all support this hypothesis. V4 has shown stronger absorption on POPG than POPC monolayers in LB experiments. FCS demonstrated that V4 disrupts POPG LUVs at a peptide:lipid ratio of 1:2. However, even at a peptide:lipid ratio of 7.5:1 no POPC vesicle disruption is observed. The data from the DPI experiments supports the observation that V4 has much greater affinity for POPG bilayers than POPC. The data in Fig. 5 shows that at an added V4 concentration of 10 μM the PG layer bound 0.44– 0.51 ng/mm^2 compared to 0.16 ng/mm^2 for PC at the same V4 concentration. The binding of V4 to PC is 19% of that compared to PG. In confocal imaging at the same peptide concentration of 25 μM, V4 showed only limited binding to POPC GUVs whereas it strongly and rapidly interacted with POPG GUVs leading to disruption. In addition, V4-TMR can be exchanged against unlabeled V4 on POPC GUVs but not on POPG GUVs. These in vitro studies with respect to the specificity of V4 provide the basis for the high selectivity in killing bacteria, but not harming mammalian cells and prove the in vivo findings of the previous study that V4 displayed a combination of high antimicrobial activity, low cytotoxic activity and low hemolytic activity with a greater specificity increase compared to polymyxin B[28].

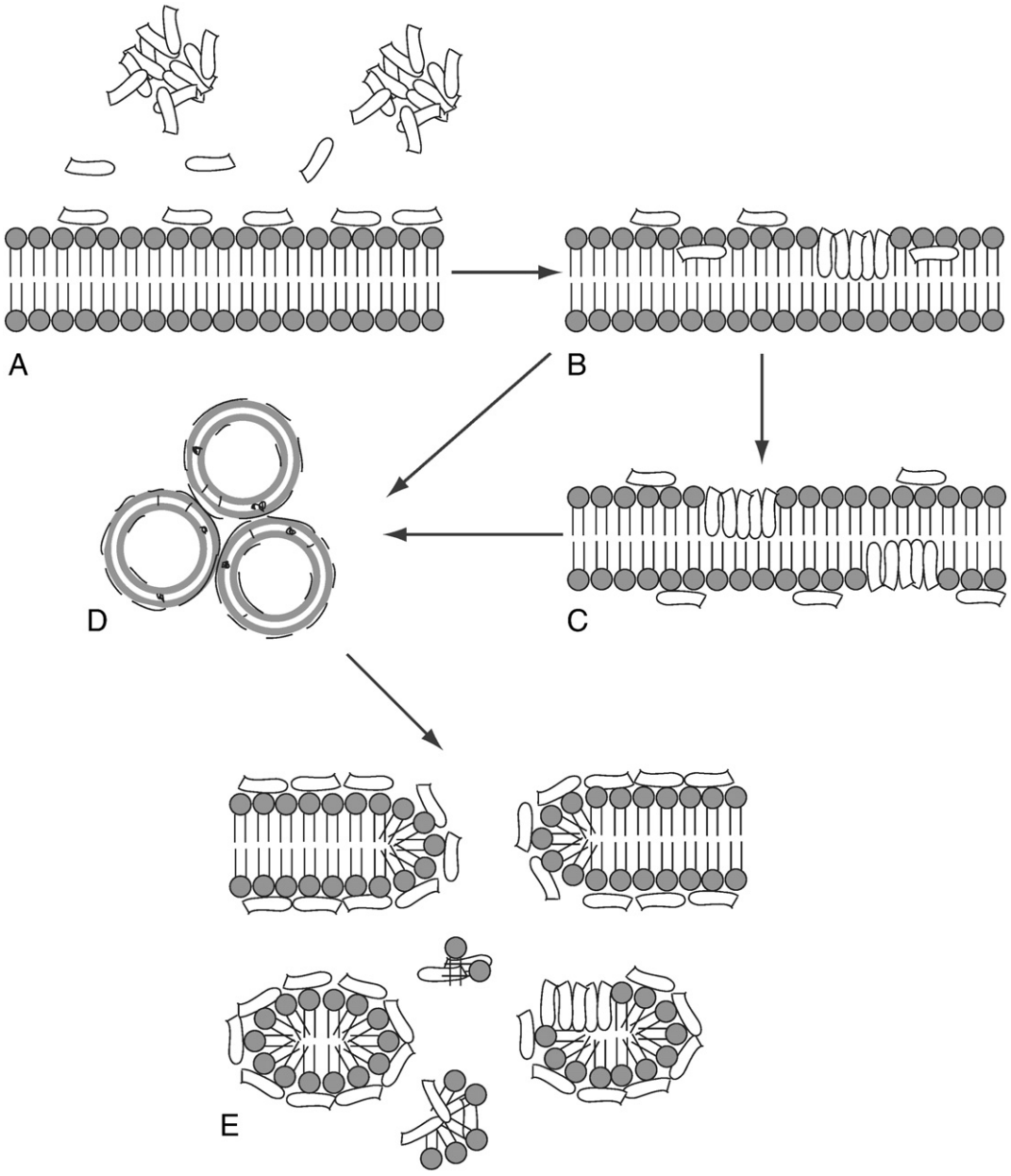

Fig. 9. Schematic drawing of the mechanism of V4 inducing membrane permeation. (A) Binding or absorption of V4 on the membrane surface. (B) Insertion of V4 into membrane and peptide aggregation. (C) Translocation of V4 into inner layer of membrane. (D) Membrane aggregation. (E) Membrane disruption. All graphs look at the bilayer in cross-section.

4.3. Effect of hydrophobic interaction

Except electrostatic forces, hydrophobic forces also contribute to V4-membrane interaction. Hydrophobic forces are important during the insertion of V4 into the membrane. Although V4 has shown stronger absorption on POPG than POPC monolayer in LB experiments, V4 also induced a considerable increase in POPC surface pressure, which is contributed by hydrophobic interactions. In AFM studies, V4 induced similar filament formation on both lipid monolayers regardless of the charge of lipid, indicating the role of hydrophobic interaction during the insertion of V4 into the hydrophobic tail groups of lipids. The isotherm studies of the premixed V4/lipid monolayer also show the role of hydrophobic interaction. For example, at 50% V4 incorporation into the mixed V4/lipid monolayer, the existence of V4 caused similar excess energy for both POPG and POPC as shown in Fig. 4. The isotherm study was done on a premixed peptide-lipid monolayer, excluding the binding or absorption process, and focused on the interaction within membranes. This result indicates that the hydrophobic interaction plays an important role during the peptide insertion into the membrane.

4.4. Membrane change induced by peptide

With increasing peptide binding, V4 begins to insert into the membrane and undergoes translocation. This process is shown by the penetration of V4 into lipid monolayers, detection of the filaments on lipid monolayer and insertion into the solid supported bilayer detected by Langmuir film balance experiments, AFM and DPI, respectively. Especially the DPI study of V4 interacting with POPG bilayers showed that V4 induced an obvious increase in bilayer mass and a concurrent decrease in layer birefringence, consistent with a significant disruption to the alignment of the lipid tails within the bilayer. Each of the concentrations of V4 (4–10 μM) induced a decrease in measured birefringence which was broadly

concentration dependent. This effect is more pronounced at the higher concentrations of V4 where the initial sharp decrease in birefringence is followed by a partial slower increase in birefringence, indicative of a re-ordering of the lipid chains to a slightly more aligned configuration following the initial chronic disruption of the lipid chain alignment induced by V4. It should be noted that the control peptide TV4, a truncated version of V4, lead neither to vesicle leakage of REVs nor to the characteristic concentration dependent change of birefringence in DPI, indicating that TV4 can bind but not penetrate into the membrane.

4.5. The role of structure of V4

As control, we have applied TV4, which has only one binding site of V4, to compare the ability of absorption and membrane disruption. TV4 has shown much lower absorption on the solid supported POPG bilayer than V4. The addition of TV4 to the POPG bilayer did not induce any change in birefringence, indicating no change in the alignment of the lipid tail. However V4 caused significant decrease in the birefringence of the POPG layer with V4 injection, suggesting a strong disruption of V4 to the alignment of the lipid chains induced by the peptide insertion. The FCS experiments also showed that TV4 did not induce any POPG vesicle leakage and disruption up to peptide: lipid ratio of 50:1, i.e. two orders of magnitude higher than the threshold for V4 action, suggesting a lack of membrane disruption ability of TV4. The difference in membrane disruption between TV4 and V4 is probably due to the structural difference between them. V4 has two binding sites (VKVQVKV) and is cyclized by an internal disulfide bond. This structure might facilitate the aggregation of peptide and perform its function. However, due to the lack of aggregation, TV4 shows no membrane disrupting ability. This result is similar to that of S3, an antimicrobial peptide from horseshoe crab. S3 dimer, which is connected by two S3 monomers through an intermolecular disulfide bond, has shown stronger ability to disrupt lipopolysaccharides (LPS) micelles and neutralize LPS activity than S3 monomer did [53]. This result is consistent with the observation that V4, which also contains a disulfide bridge, shows membrane activity, while TV4 does not. Therefore the disulfide bond and possibly more so the multiplicity of endotoxin binding sites might play important roles in peptide function.

5. Conclusion

Antimicrobial peptides are important potential antimicrobial drugs and therefore the investigation of new peptide design and their mechanisms acting on the membrane are subjects which have elicited great interest. In this work, we have demonstrated the combination of several approaches to examine the interaction of an artificial novel antimicrobial peptide, V4, with different membrane mimics to unravel the mechanism of this interesting peptide which has shown high specificity and antimicrobial activity for some microbes. This study provided the in vitro proof for the high selectivity of V4. Electrostatic interaction and hydrophobic interaction have different functions during antimicrobial interaction. Electrostatic forces provide selectivity and affinity to allow peptide accumulation on the membrane above the surface concentration threshold above which hydrophobic forces lead to insertion of V4 into the membrane. The existence of a surface concentration threshold suggests that the peptide integrates in an oligomeric or aggregated form. However, due to the neutralization of charges during binding and the very strong hydrophobicity of V4, the peptide leads as well to vesicle aggregation before vesicle disruption takes place. While this effect can be desirable when agglutination reduces bacterial growth, it is not essential since immobilized vesicles can be disrupted without any vesicle aggregation. In addition, it would be advantageous to reduce V4 hydrophobicity to increase peptide solubility [29]. This study enhances the understanding of the predominant specificity of V4 and the mode of action on membranes, and contributes to the rational design of novel antimicrobial peptides, by suggesting the predominant contribution of different amino acids to the action mechanism [54].

Acknowledgements

The research in this work was funded by NUS grant R-143-000-338-112. LY acknowledges support by a NUS graduate scholarship.

References

[1] M. Zasloff, Antimicrobial peptides of multicellular organisms, Nature 415 (2002) 389–395.
[2] M. Stark, L.P. Liu, C.M. Deber, Cationic hydrophobic peptides with antimicrobial activity, Antimicrob. Agents Chemother. 46 (2002) 3585–3590.
[3] R.E.W. Hancock, R. Lehrer, Cationic peptides: a new source of antibiotics, Trends Biotechnol. 16 (1998) 82–88.
[4] K.L. Brown, R.E. Hancock, Cationic host defense (antimicrobial) peptides, Curr. Opin. Immunol. 18 (2006) 24–30.
[5] J.B. McPhee, R.E. Hancock, Function and therapeutic potential of host defence peptides, J. Pept. Sci. 11 (2005) 677–687.
[6] A. Tossi, L. Sandri, A. Giangaspero, Amphipathic, alpha-helical antimicrobial peptides, Biopolymers 55 (2000) 4–30.
[7] K.A. Brogden, M. Ackermann, J. McCray, B.F. Tack, Antimicrobial peptides in animals and their role in host defences, Int. J. Antimicrob. Agents 22 (2003) 465–478.
[8] P. Bulet, C. Hetru, J.L. Dimarcq, D. Hoffmann, Antimicrobial peptides in insects; structure and function, Dev. Comp. Immunol. 23 (1999) 329–344.
[9] S.K. De, R. Contreras, Human antimicrobial peptides: defensins, cathelicidins and histatins, Biotechnol. Lett. 27 (2005) 1337–1347.
[10] M. Zasloff, Magainins, a class of antimicrobial peptides from Xenopus skin: isolation, characterization of two active forms, and partial cDNA sequence of a precursor, Proc. Natl. Acad. Sci. USA 84 (1987) 5449–5453.
[11] M. Zasloff, B. Martin, H.C. Chen, Antimicrobial activity of synthetic magainin peptides and several analogues, Proc. Natl. Acad. Sci. USA 85 (1988) 910–913.
[12] F.L. Schuster, L.S. Jacob, Effects of magainins on ameba and cyst stages of Acanthamoeba polyphaga, Antimicrob. Agents Chemother. 36 (1992) 1263–1271.
[13] L.H. Kondejewski, S.W. Farmer, D.S. Wishart, R.E.W. Hancock, R.S. Hodges, Gramicidin S is active against both gram-positive and gram-negative bacteria, Int. J. Pept. Protein Res. 47 (1996) 460–466.
[14] E.J. Prenner, R.N.A.H. Lewis, R.N. McElhaney, The interaction of the antimicrobial peptide gramicidin S with lipid bilayer model and biological membranes, Biochim. Biophys. Acta 1462 (1999) 201–221.
[15] H.G. Boman, D. Wade, I.A. Boman, B. Wahlin, R.B. Merrifield, Antibacterial and antimalarial properties of peptides that are cecropin-melittin hybrids, FEBS Lett. 259 (1989) 103–106.
[16] D.G. Lee, Y. Park, I. Jin, K.S. Hahm, H.H. Lee, Y.H. Moon, E.R. Woo, Structure-antiviral activity relationships of cecropin A-magainin 2 hybrid peptide and its analogues, J. Pept. Sci. 10 (2004) 298–303.
[17] L.H. Kondejewski, S.W. Farmer, D.S. Wishart, C.M. Kay, R.E.W. Hancock, R.S. Hodges, Modulation of structure and antibacterial and hemolytic activity by ring size in cyclic gramicidin S analogs, J. Biol. Chem. 271 (1996) 25261–25268.
[18] L.H. Kondejewski, M. Jelokhani-Niaraki, S.W. Farmer, B. Lix, C.M. Kay, B.D. Sykes, R.E. Hancock, R.S. Hodges, Dissociation of antimicrobial and hemolytic activities in cyclic peptide diastereomers by systematic alterations in amphipathicity, J. Biol. Chem. 274 (1999) 13181–13192.
[19] H. Keun Kim, D. Gun Lee, Y. Park, H. Nam Kim, B. Hwa Choi, C.H. Choi, K.S. Hahm, Antibacterial activities of peptides designed as hybrids of antimicrobial peptides, Biotechnol. Lett. 24 (2002) 347–353.
[20] Y. Park, D.G. Lee, K.S. Hahm, HP(2–9)-magainin 2(1–12), a synthetic hybrid peptide, exerts its antifungal effect on Candida albicans by damaging the plasma membrane, J. Pept. Sci. 10 (2004) 204–209.
[21] S.A. Muhle, J.P. Tam, Design of Gram-Negative Selective Antimicrobial Peptides, Biochemistry 40 (2001) 5777–5785.
[22] C. Landon, F. Barbault, M. Legrain, M. Guenneugues, F. Vovelle, Rational design of peptides active against the gram positive bacteria Staphylococcus aureus, Proteins 72 (2008) 229–239.
[23] C.R.H. Raetz, C. Whitfield, Lipopolysaccharide endotoxins, Ann. Rev. Biochem. 71 (2002) 635–700.
[24] Y. Rosenfeld, N. Papo, Y. Shai, Endotoxin (LPS) neutralization by innate immunity host-defense peptides: Peptides' properties and plausible modes of action, J. Biol. Chem. 281 (2006) 1636–1643.
[25] N.S. Tan, B. Ho, J.L. Ding, High-affinity LPS binding domain(s) in recombinant factor C of a horseshoe crab neutralizes LPS-induced lethality, FASEB J. 14 (2000) 859–870.
[26] C. Erridge, E. nett-Guerrero, I.R. Poxton, Structure and function of lipopolysaccharides, Microbes. Infect. 4 (2002) 837–851.
[27] V. Frecer, B. Ho, J.L. Ding, Interpretation of biological activity data of bacterial endotoxins by simple molecular models of mechanism of action, Eur. J. Biochem. 267 (2000) 837–852.
[28] V. Frecer, B. Ho, J.L. Ding, De Novo Design of Potent Antimicrobial Peptides, Antimicrob. Agents Chemother. 48 (2004) 3349–3357.

[29] L. Yu, J.L. Ding, B. Ho, T. Wohland, Investigation of a novel artificial antimicrobial peptide by fluorescence correlation spectroscopy: an amphipathic cationic pattern is sufficient for selective binding to bacterial type membranes and antimicrobial activity, Biochim. Biophys. Acta 1716 (2005) 29–39.
[30] L. Yu, J.L. Ding, B. Ho, S.S. Feng, T. Wohland, Investigation of the mechanisms of antimicrobial peptides interacting with membranes by fluorescence correlation spectroscopy, The Open Chemical Physics Journal 1 (2008) 62–80.
[31] L.Y. Zhao, S.S. Feng, Effects of lipid chain length on molecular interactions between paclitaxel and phospholipid within model biomembranes, J. Colloid. Interface Sci. 274 (2004) 55–68.
[32] L.Y. Zhao, S.S. Feng, M.L. Go, Investigation of molecular interactions between paclitaxel and DPPC by Langmuir film balance and differential scanning calorimetry, J. Pharm. Sci. 93 (2004) 86–98.
[33] G.H. Cross, A.A. Reeves, S. Brand, J.F. Popplewell, L.L. Peel, M.J. Swann, N.J. Freeman, A new quantitative optical biosensor for protein characterisation, Biosens. Bioelectron 19 (2003) 383–390.
[34] G.H. Cross, G.H. Cross, Y. Ren, Y. Ren, N.J. Freeman, N.J. Freeman, Young's fringes from vertically integrated slab waveguides: applications to humidity sensing, J. Appl. Phys. 86 (1999) 6483–6488.
[35] R.S. Marks, C.R. Lowe, D.C. Cullen, H.H. Weetall, I. Karube, Handbook of biosensors and biochip, Wiley-Interscience, UK, 2007.
[36] G.H. Cross, A. Reeves, S. Brand, M.J. Swann, L.L. Peel, N.J. Freeman, J.R. Lu, The metrics of surface adsorbed small molecules on the Young's fringe dual-slab waveguide interferometer, J. Phys. D: Appl. Phys. (2004) 74–80.
[37] R. Horvath, J.J. Ramsden, Quasi-isotropic analysis of anisotropic thin films on optical waveguides, Langmuir 23 (2007) 9330–9334.
[38] J.F. Nagle, S. Tristram-Nagle, Structure of lipid bilayers, Biochim. Biophys. Acta 1469 (2000) 159–195.
[39] A. Mashaghi, M. Swann, J. Popplewell, M. Textor, E. Reimhult, Optical anisotropy of supported lipid structures probed by waveguide spectroscopy and its application to study of supported lipid bilayer formation kinetics, Anal. Chem. 80 (2008) 3666–3676.
[40] H.M. McConnell, T.H. Watts, R.M. Weis, A.A. Brian, Supported planar membranes in studies of cell–cell recognition in the immune system, Biochim. Biophys. Acta 864 (1986) 95–106.
[41] D. Madge, Chemical kinetics and fluorescence correlation spectroscopy, Q. Rev. Biophys. 9 (1976) 35–47.
[42] J. Widengren, R. Rigler, Fluorescence correlation spectroscopy as a tool to investigate chemical reactions in solutions and on cell surfaces, Cell. Mol. Biol. 44 (1998) 857–879.
[43] M. Ehrenberg, R. Rigler, Rotational brownian motion and fluorescence intensify fluctuations, Chem. Phys. 4 (1974) 390–401.
[44] O. Krichevsky, G. Bonnet, Fluorescence correlation spectroscopy: the technique and its applications, Rep. Prog. Phys. 65 (2002) 251–297.
[45] K. Bacia, S.A. Kim, P. Schwille, Fluorescence cross-correlation spectroscopy in living cells, Nat. Meth. 3 (2006) 83–89.
[46] D. Magde, E.L. Elson, W.W. Webb, Fluorescence correlation spectroscopy. II. An experimental realization, Biopolymers 13 (1974) 29–61.
[47] R. Rigler Mets, J. Widengren, P. Kask, Fluorescence correlation spectroscopy with high count rate and low background: analysis of translational diffusion, Eur. Biophys. J. 22 (1993) 169–175.
[48] P. Kask, R. Günther, P. Axhausen, Statistical accuracy in fluorescence fluctuation experiments, Eur. Biophys. J. 25 (1997) 163–169.
[49] U. Meseth, T. Wohland, R. Rigler, H. Vogel, Resolution of fluorescence correlation measurements, Biophys. J. 76 (1999) 1619–1631.
[50] T. Wohland, R. Rigler, H. Vogel, The standard deviation in fluorescence correlation spectroscopy, Biophys. J. 80 (2001) 2987–2999.
[51] Y. Sato, N. Ishikawa, T. Takagi, High-performance size-exclusion chromatography and molar mass measurement by low-angle laser light scattering of recombinant yeast-derived human hepatitis B virus surface antigen vaccine particles, J. Chromatogr. 507 (1990) 25–31.
[52] A. Pramanik, P. Thyberg, R. Rigler, Molecular interactions of peptides with phospholipid vesicle membranes as studied by fluorescence correlation spectroscopy, Chem. Phys. Lipids 104 (2000) 35–47.
[53] P. Li, T. Wohland, B. Ho, J.L. Ding, Perturbation of Lipopolysaccharide (LPS) Micelles by Sushi 3 (S3) antimicrobial peptide: the importance of an intermolecular disulfide bond in S3 dimer for binding, disruption, and neutralization of LPS, J. Biol. Chem. 279 (2004) 50150–50156.
[54] V. Frecer, QSAR analysis of antimicrobial and haemolytic effects of cyclic cationic antimicrobial peptides derived from protegrin-1, Bioorg. Med. Chem. 14 (2006) 6065–6074.
[55] T. Plenat, S. Deshayes, S. Bolchot, P.E. Milhiet, R.B. Cole, F. Heitz, C.L. Grimellec, Interaction of primary amphipathic cell-penetrating peptides with phospholipids supported monolayers, Langmuir 20 (2004) 9255–9261.